



HAL
open science

Major non-volatile intermediate products of photo-catalytic decomposition of ethylene

Siteng Tieng, Zixian Jia, Sana Labidi, Ana Paola Diaz-Gomez Trevino, Pierre Eloy, Eric M. Gaigneaux, Khay Chhor, Andreï Kanaev

► To cite this version:

Siteng Tieng, Zixian Jia, Sana Labidi, Ana Paola Diaz-Gomez Trevino, Pierre Eloy, et al.. Major non-volatile intermediate products of photo-catalytic decomposition of ethylene. *Chinese Journal of Catalysis*, 2019, 374, pp.328-334. 10.1016/j.jcat.2019.05.008 . hal-02405814

HAL Id: hal-02405814

<https://hal.science/hal-02405814>

Submitted on 25 Oct 2021

HAL is a multi-disciplinary open access archive for the deposit and dissemination of scientific research documents, whether they are published or not. The documents may come from teaching and research institutions in France or abroad, or from public or private research centers.

L'archive ouverte pluridisciplinaire **HAL**, est destinée au dépôt et à la diffusion de documents scientifiques de niveau recherche, publiés ou non, émanant des établissements d'enseignement et de recherche français ou étrangers, des laboratoires publics ou privés.



Distributed under a Creative Commons Attribution - NonCommercial 4.0 International License

1 Major non-volatile intermediate products of
2 photo-catalytic decomposition of ethylene

3

4 Siteng Tieng¹, Zixian JIA^{1#}, Sana Labidi¹, Ana Paola Diaz-Gomez Trevino¹, Pierre Eloy²,
5 Eric Gaigneaux², Khay Chhor¹, Andrei Kanaev¹

6

7 ¹*Laboratoire des Sciences des Procédés et des Matériaux, CNRS, Université Paris 13, Sorbonne Paris*
8 *Cité, Villetaneuse, France*

9 ²*Université Catholique de Louvain, Unité de catalyse et chimie des matériaux diverses, Louvain-la-*
10 *Neuve, Belgium*

11

12

Corresponding Author
E-mail Address: zixian.jia@lspm.cnrs.fr

13 **Abstract**

14 A complex kinetics of the photocatalytic decomposition of gaseous ethylene on nanoparticulate Fe(III)
15 doped anatase TiO₂ was analyzed in a continuous-flow fixed-bed reactor. The analysis evidenced the
16 production of non-volatile intermediate reaction products, which cover the photocatalyst surface and
17 delay the time of attaining the stationary reactor performance. As a result, the reaction yield slowly
18 increases during the long-lasting (~3 hours) intermediate stage. Based on Raman, FTIR and thermal
19 post-treatment analyses, we assigned the major non-volatile reaction product to polymeric oxidized
20 hydrocarbons: furan and furfural oligomers. A theoretical model is proposed explaining the observed
21 kinetics.

22

23

24

25 *Key words: Photocatalysis, process kinetics, Fe-doped TiO₂ nanoparticles, ethylene, non-volatile*
26 *products, polyfuran, polyfurfural*

27

28

29

30 I. Introduction

31 Photocatalysis in the gas phase has attracted much attention during recent years because of its
32 wide potential for air purification. The most commonly used photocatalyst is titanium dioxide (TiO₂)
33 known for its photocorrosion resistance and low cost. The photocatalytic activity of this material is
34 due to the generation of the electron–hole pair under UV light illumination. However, the major
35 problem that restraints its industrial implementation is related to low quantum yield of the
36 photooxidation reactions [1]. Cationic and anionic doping of TiO₂ is one of the typical approaches to
37 enhance photocatalytic efficiency under UV light illumination. Researchers have investigated the
38 effects of transition metal such as iron [2–4], which is much cheaper than noble metal such as Ag [5]
39 and Au [6] on reducing band gaps, decreasing electron and hole recombination rate, and using visible
40 light.

41 The heterogeneous photocatalysis generally involves intermediate reaction products, which
42 desorption and reactivity affect the overall process efficiency. Their knowledge is of particular
43 importance for the process optimization and rigorous comparison of the material activities. Between
44 different pollutants, ethylene is often considered as the model one because of its seemingly simple
45 decomposition scheme involving few intermediate reaction products. In the same time, the ethylene
46 abatement remains one of important environmental tasks. The photocatalytic oxidation of ethylene has
47 been largely reported in literature [7–11]. Several studies have addressed intermediate products of the
48 ethylene photodegradation. Bhattacharyya et al. [12] have observed formic acid as the main by-
49 product, while Wang et al. [13] have reported on the formation of aldehydes and alcohols. Einaga and
50 Teraoka [14] have analyzed the ethylene photooxidation on TiO₂ doped with platinum. In the absence
51 of water vapor, absorption bands in the range of 1200–1800 cm⁻¹ have been observed and attributed to
52 oxygenated compounds containing C–O, COO⁻ and C=O groups. The concentration of these
53 intermediate species decreases with the irradiation time in presence of water vapors, leading to their
54 complete mineralization into CO₂. Several studies [15–17] have reported on the formation of ethane
55 C₂H₆, while oxygenated hydrocarbons CH₃CHO, CH₃COCH₃ and CH₃COC₂H₅ were present in a small
56 quantity. In the same time, non-volatile reaction products, capable remaining on the catalyst surface

57 and affecting the process kinetics and reaction yield, have not been investigated in previous studies,
58 probably because of their not easy detection.

59 Previously, we have reported on the effective ethylene decomposition using nanoparticulate TiO₂
60 coatings homogeneously doped with Fe(III) [18,19]. A net difference in the photocatalytic kinetics
61 between the first and subsequent reactor runs has been observed on the initial process stage, which
62 could be related to a participation of unknown reaction products. In the present communication we
63 report on the kinetics analysis of gaseous ethylene photocatalytic decomposition on nanoparticulate
64 Fe(III) doped anatase titania. We assign major non-volatile reaction products and provide a theoretical
65 model explaining their influence on the reaction kinetics.

66

67 **II. Experimental methods**

68 2.1 Sample preparation

69 The Fe(III)-doped TiO₂ anatase photocatalyst with the optimal composition was used in this work
70 because of its higher reaction efficiency compared with a pure titania. The preparation procedure has
71 been described in our previous works [18,19]. In short, the material was obtained in the two-stage
72 process including (1) fabrication, doping and immobilization on a glass support of titanium-oxo-
73 alkoxy (TOA) nanoparticles, followed by (2) thermal treatment of the nanoparticulate coating. The
74 doping of TOA nanoparticles with Fe³⁺ ions was achieved at the nucleation stage. The homogeneity of
75 the coating doping has been evidenced in the previous studies. The colloids have been prepared using
76 hydrolysis ratio H= 2.0, which corresponds to one of the stability domains of the TOA sol–gel process
77 and enables metastable chemically active monodispersed nanoparticles of size 2R=5.2 nm. The
78 concentration of iron in TiO₂ was fixed to 0.005 mol%, which corresponds to the best photocatalytic
79 activity of the coating [19]. The reactive colloid has been set in a short contact with the supporting
80 material, preliminary treated with 95 mol% sulfuric acid at 70 °C for 4 hours and washed in ultrasound
81 bath. The beads with the deposited photocatalyst were heat treated at 500 °C for 4 hours to obtain
82 anatase crystalline phase.

83 For the synthesis, analytical grade reagents and distilled water were used. Iron (III)
84 acetylacetonate of 99.9% purity was supplied by Sigma–Aldrich. Titanium tetraisopropoxide (TTIP) and
85 2-propanol with respectively 98% and 99.5% purity were purchased from Acros Organics.

86

87 2.2 Sample characterization

88 The Fe(III)-doped TiO₂ anatase photocatalyst preparation was previously reported by our group
89 [18,19]. The characterization of catalyst was summarized in supporting information. From Fig. S1, it
90 is observed that the surface with mean roughness of ~0.5 nm and composed of agglomerates formed
91 by particles of average size $\sim 6 \pm 3$ nm which was also evidenced by TEM image (Fig. S1). The XRD
92 (Fig. S3) indicates that Fe(III)–TiO₂ powder well crystallizes in the anatase phase in the considered
93 temperature range. Fig.S4 displays XPS spectra of the doped samples in two relevant energy ranges of
94 450-470eV and 530-540eV. In agreement with studies of pure TiO₂, photoemission bands appearing at
95 464.5 ± 0.2 eV and 458.7 ± 0.2 eV can be attributed to Ti 2p^{1/2} and Ti 2p^{3/2} states of Ti⁴⁺ and the signal
96 associated with singlet oxygen was also observed at 530.0 ± 0.4 eV with a shoulder at 531.5 ± 0.3 eV.
97 Fig.S5 shows typical XPS spectrum of our Fe(III)-TiO₂ coatings in the energy range 700-
98 745eV. Because of the low Fe concentration, two weak signals were observed at 709.9 eV and 723.5
99 eV as well as the satellites of a very low intensity.

100

101 2.3. Photocatalytic experiments

102 The experimental conditions are listed in Table 1.

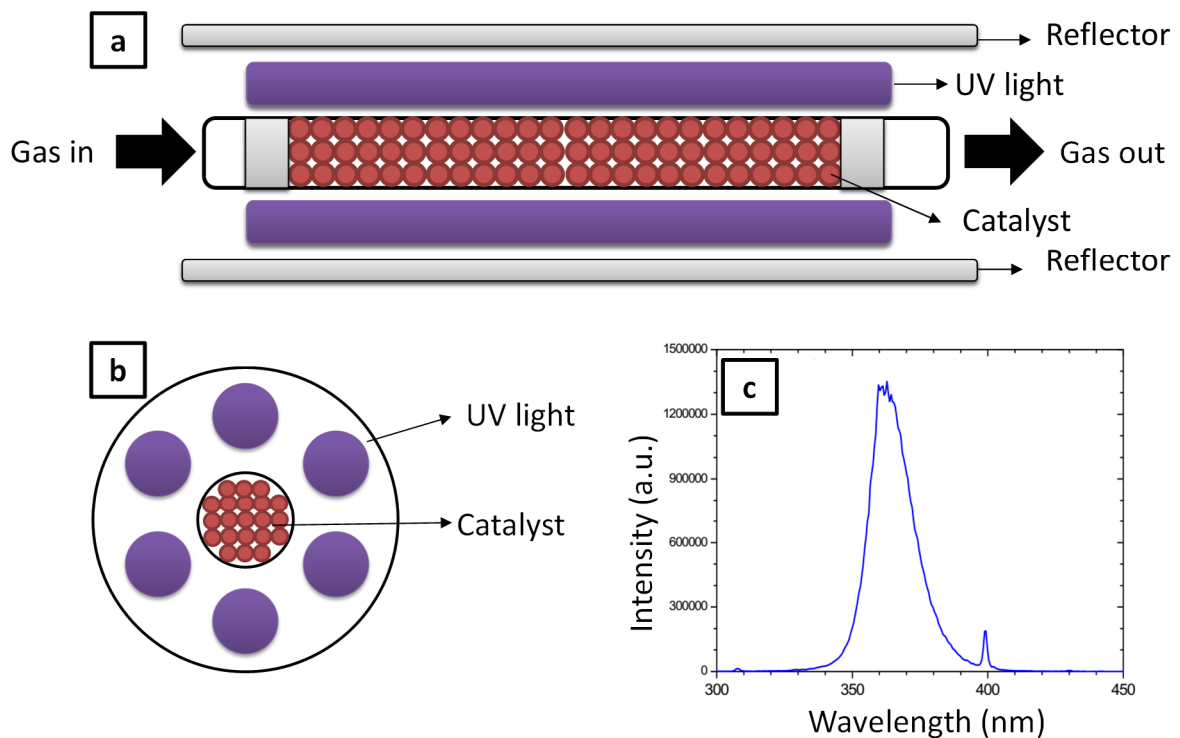
103 Table 1: Experimental conditions of photocatalytic experiments

Gas mixture flow rate	90 ml/min
Reactor length	30 cm
Photocatalyst mass	6,6 mg
Ethylene concentration	34 ppm
Relative humidity R _H	13 %
Pollutant residence time in the reactor tube	1,4 s

104

105 The photocatalytic experiments were performed with a laboratory gas-phase continuous flow
106 fixed-bed reactor depicted in Fig.1. In short, air gas flow containing pollutant and water vapour passes

107 through the reactor tube made of transparent glass in the UVA spectral region of $\lambda \geq 320$ nm. The
 108 reactor tube of 6 mm diameter is surrounded by six 8-W lamps emitting at 362 nm ($\Delta\lambda_{\text{hwfm}} = 22$ nm).
 109 Ethylene concentrations before (C_{in}) and after (C_{out}) the reactor tube were analysed by a gas
 110 chromatography device (Varian CP 3800) equipped with two injection loops allowing measurements
 111 in a continuous sampling mode. The temperature of the photocatalytic bed was continuously
 112 monitored. The pollutant conversion (or reactor yield) is calculated according to $\eta(\%) = 100 \cdot (1 -$
 113 $C_{\text{out}}/C_{\text{in}})$.



114
 115 **Figure 1.** (a) Cut section and (b) cross section of the photocatalytic reactor and (c) Emission
 116 spectrum of the UV light.

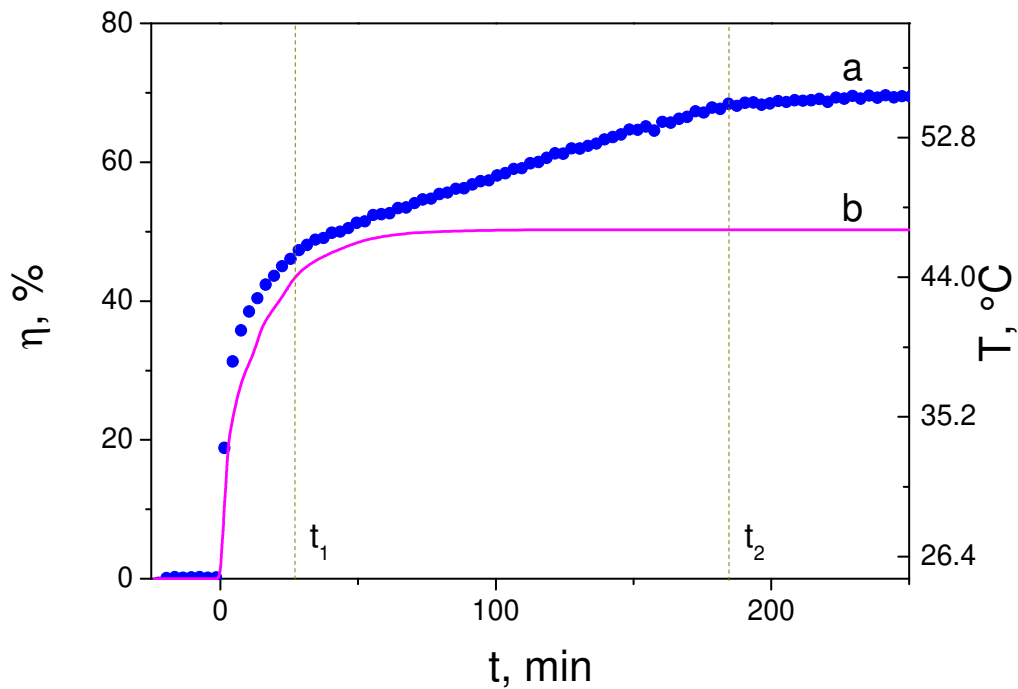
117

118 III. Results and discussion

119 3.1 Intermediate reaction products

120 The ethylene conversion kinetics over the freshly prepared photocatalyst shows three main stages
 121 as depicted in Fig. 2a. (1) On the first stage $0 \leq t \leq t_1$ ($t=0$ corresponds to illumination of the reactor
 122 lamps), the ethylene conversion increases rapidly, which corresponds to the temperature increase
 123 (curve b in Fig. 2) that may thermally activate photocatalytic reactions. (2) The second stage taking

124 significantly long time $t_1 \leq t \leq t_2$ consists in a slow increase of the ethylene conversion, which is
125 apparently controlled by the surface chemistry and reactive interface modification. (3) At the end of
126 the second stage, the stationary regime is attained. This maximum stationary activity of the
127 photocatalyst keeps over week without any signs of deactivation.

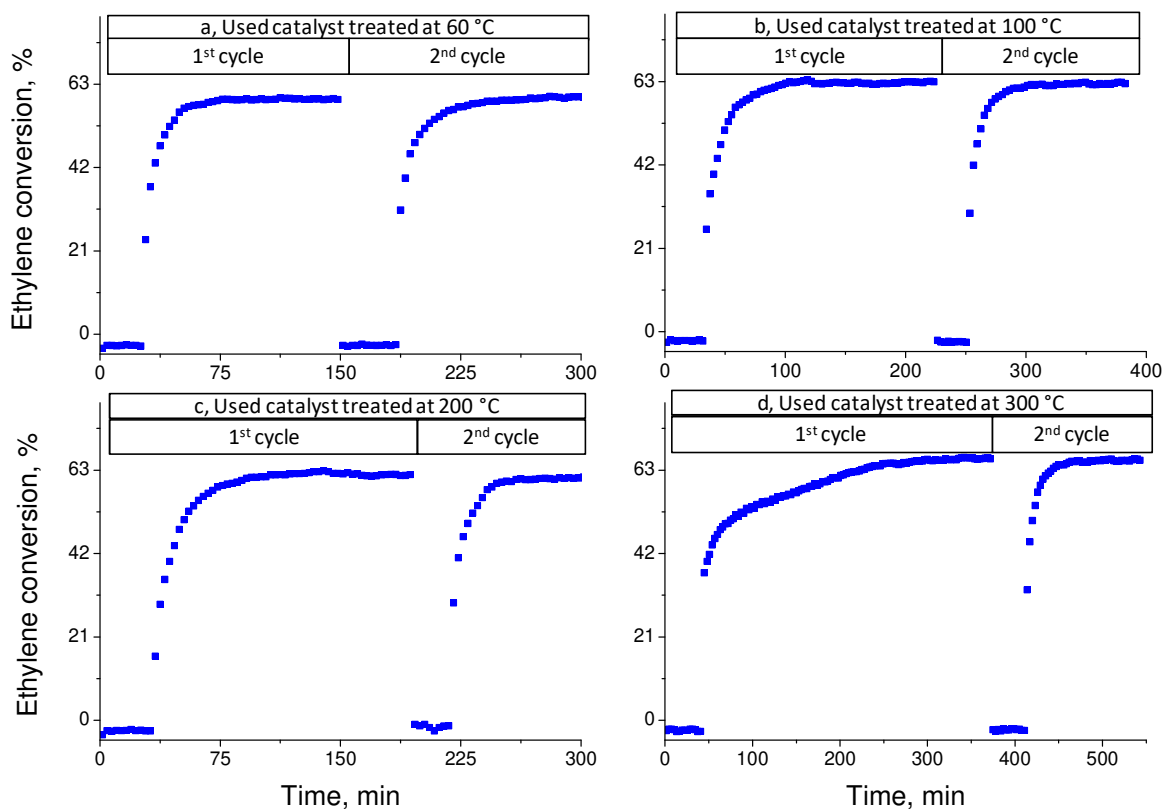


128

129 **Figure 2.** Ethylene conversion η (a) and temperature (b) of a fixed-bed continuous-flow
130 photocatalytic reactor.

131 The slow intermediate stage 2 was only observed with the freshly prepared photocatalyst. This
132 stage was absent with the reused material where the pollutant conversion rapidly attained the
133 maximum level. The strong increase (almost twice) of the process efficiency during stage 2 suggests
134 significant modification of the reactive interface that can be related to the accumulation of reaction
135 products. Apparently, the known acetaldehyde [20] or CO_2 -CO [21] cannot be candidates since do not
136 accelerate the decomposition kinetics and may only slow it down by closing the active surface sites. In
137 the same time, the gas chromatography analysis at the reactor exit did not evidence any significant
138 traces of new products except for ethylene, CO/CO_2 and water. It is assumed therefore that the major
139 kinetics modification at this stage is due to an unknown non-volatile product accumulated at the
140 photocatalyst surface.

141 In order to confirm the presence of non-volatile intermediate products, accumulated during the
142 transitory stage 2, photocatalyst already used in the process (which don't manifest the transitory stage
143 and rapidly attains stationary performance) was exposed to a secondary thermal treatment. Such heat
144 treatment under ambient air is expected to sublimate or burn the deposited species that converts the
145 reactive interface to its original state. The photocatalytic test was performed after the secondary heat
146 treatment in order to check if the reaction kinetics recovers. The results are shown in Fig. 3 the
147 photocatalysts heat treated at temperatures (a) 60 °C for 3 hours under UV illumination (this reference
148 series reproduces the reactor conditions), (b) 100 °C for 3 hours, (c) 200 °C for 3 hours and (d) 300 °C
149 for 1 hour. One can see that the used photocatalysts exposed to temperatures $T \leq 200$ °C (Fig. 3a,b,c) do
150 not regain the original kinetics, while that exposed to $T=300$ °C (Fig. 3d) restores kinetics of the
151 freshly prepared material. These results indicate that the intermediates product involved in the
152 photocatalytic process of ethylene decomposition has relatively high stability against desorption at the
153 photocatalyst surface. Previous DSC-TGA measurements have evidenced the departure of the
154 adsorbed alcohol and water at temperatures ~ 80 °C [22], which indicates that, the surface species are
155 much heavier in our case. Consequently, it was suggested that the intermediate reaction products of
156 the ethylene decomposition are strongly bound to the surface. Commonly, the temperature range 200
157 $^{\circ}\text{C} < T \leq 300$ °C corresponds to the burning of surface organics [23]. It is concluded therefore that
158 photocatalytic decomposition of ethylene includes as an intermediate step the formation of stable non-
159 volatile products at the photocatalyst surface.

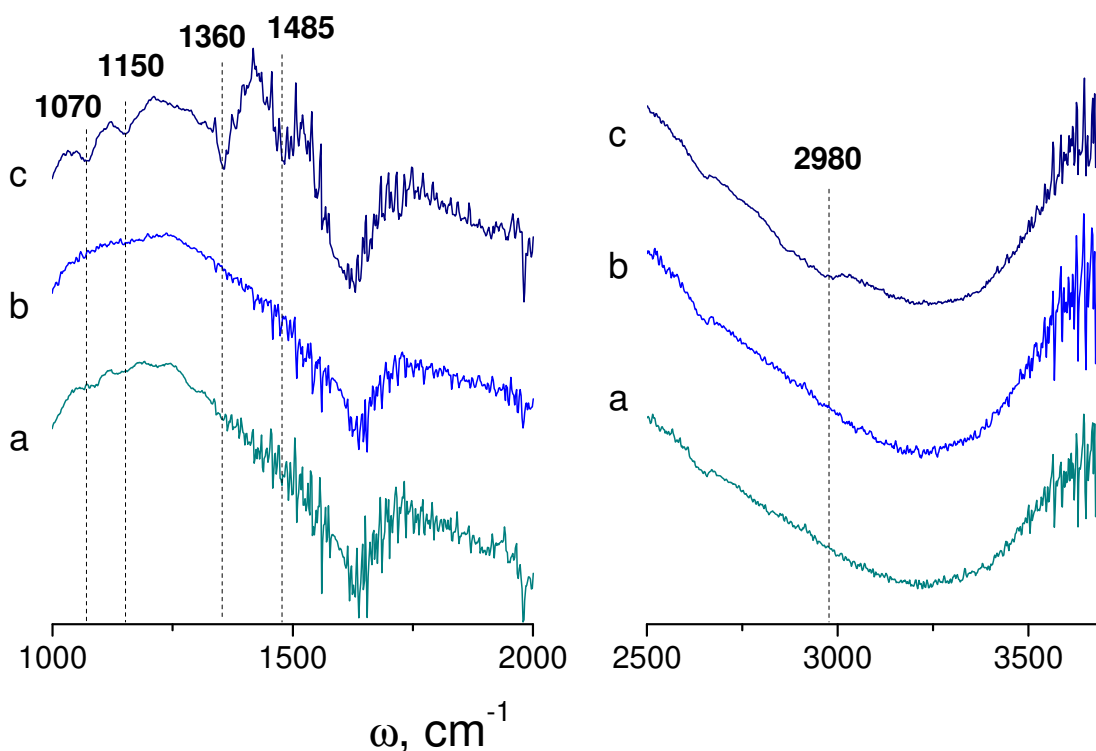


160

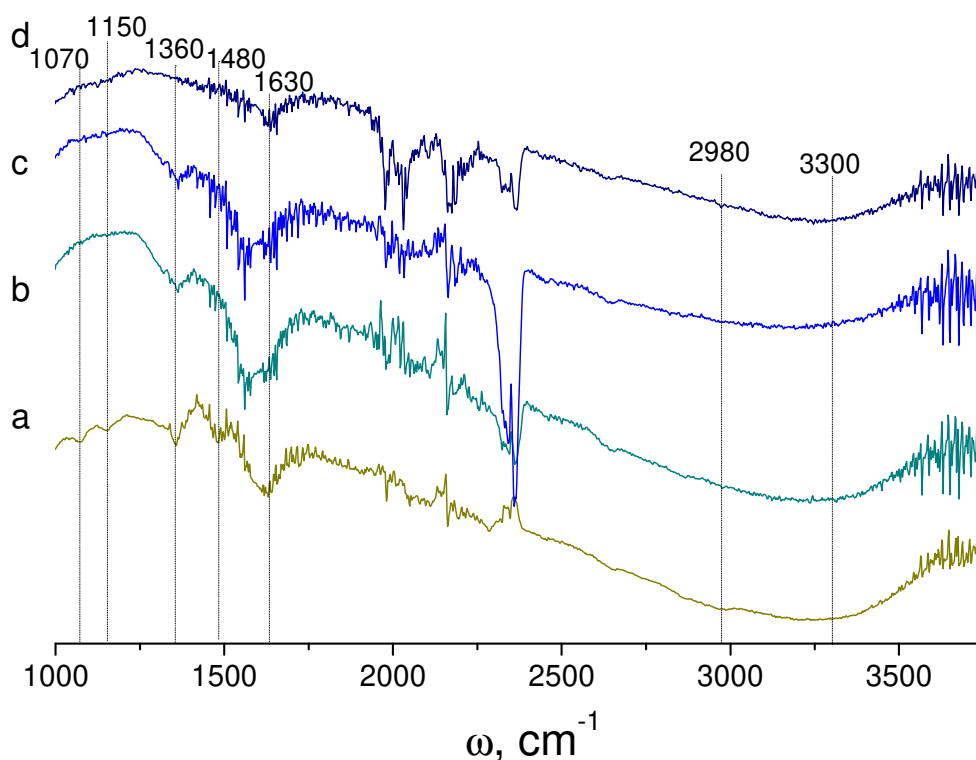
161 **Figure 3.** Ethylene conversion of used Fe(III)-TiO₂ photocatalyst subsequently heat treated in a
 162 dry air flow: (a) at 60°C during 3hours under UVA illumination, (b) at 100°C during 3
 163 hours,(c) at 200°C during 3 hours and d) at 300°C during 1 hour. (Each photocatalyst
 164 has been studied in two repeated cycles).

165 In order to clarify the nature of these intermediate species, the FTIR analysis of the photocatalyst
 166 was performed after utilisation in the reactor. Fig. 4 displays IR spectra in frequency ranges of 1000-
 167 2000 cm⁻¹ and 2400-4000 cm⁻¹ of the freshly prepared catalyst (a) and that kept in the reactor under the
 168 pollutant flow during 10 hours with the UVA lamps off (b) and on (c). The presence of the adsorbed
 169 species at the catalyst surface was evidenced the appearance of absorption bands at 1070, 1150, 1360,
 170 1480, and 2980 cm⁻¹ in spectrum (c), in contrast to those of freshly prepared photocatalyst (a) and that
 171 exposed to the pollutant without UVA illumination (b) which look similar. Complimentary, FTIR
 172 spectra was measured with the used photocatalyst submitted to the secondary thermal treatment, as in
 173 the process kinetics measurements previously discussed in Fig. 3. The results are presented in Fig. 5.
 174 In agreement with the previous conclusion, the absorption bands of the adsorbed species at 1070,
 175 1150, 1360, 1480, and 2980 cm⁻¹ (a-b) began to change after heating at 200 °C (c) and completely

176 disappear after being exposed to the temperature of 300 °C (d). This observation is consistent with the
 177 burning of organics chemically bound to the photocatalyst surface. The following assignment for the
 178 observed IR bands can be proposed. The large band around 3300 cm⁻¹ belongs to O-H stretching mode
 179 of physisorbed water, surface hydroxyl groups and/or hydroxyl groups of by-product and the band at
 180 1630 cm⁻¹ is associated with O-H deformation mode. The weak band at about 2980 cm⁻¹ is due to
 181 stretching vibration $\nu(\text{CH})$ and the band at 1480 cm⁻¹ is due to deformation vibration $\delta(\text{CH}_2)$. The band
 182 located around 1360 cm⁻¹ can be attributed to the deformation vibration modes $\delta(\text{OH})+\delta(\text{CH}_2)$ [24].
 183 The relatively weak bands appearing at 1150 and 1070 cm⁻¹ were tentatively assigned to the
 184 deformation vibration $\delta(\text{CH}_2)$ and antisymmetric stretching $\nu(\text{C-O})$ [25] of alcohols. As mentioned
 185 above, several authors have reported the presence of carbonyl intermediates such as CH₃CHO,
 186 CH₃COCH₃ or CH₃COC₂H₅ [24,26,27]. In this work, the absence of the absorption band at 1700cm⁻¹
 187 allows to reject the presence of carbonyl derivatives as intermediates.



188
 189 **Figure 4.** FTIR spectra of Fe(III)-TiO₂ photocatalyst (a) freshly prepared, (b) freshly prepared
 190 after being exposed to gaseous ethylene flow in dark for 3 hours and (c) after UVA
 191 illumination in presence of pollutant for 3 hours.



192

193

194 **Figure 5.** FTIR spectra of Fe(III)-TiO₂ photocatalyst: freshly prepared (a) and used after
 195 secondary thermal treatment for 1 hour at 100°C (b), 200 °C (c) and 300°C (d).

196

197

198

199

200

201

202

203

204

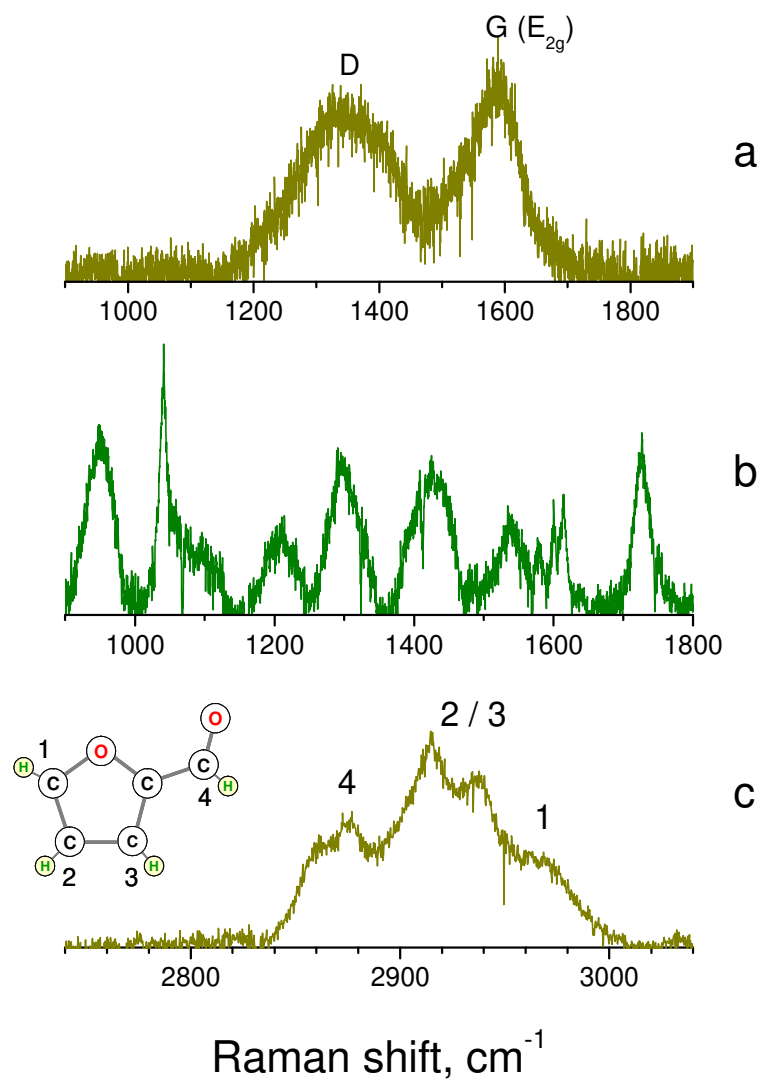
205

206

207

208

Several studies have been reported in the past on organic photopolymerization in presence of semiconducting solids. Popović et al. [28] have observed polymerization of methacrylic acid on CdS, CdS/HgS and CdS/TiO₂ triggered by free holes photogenerated in valence band. Damm et al. [29] have compared UV photopolymerization of methyl tri-acrylate with P25-TiO₂ and anatase TiO₂ prepared by spray-hydrolysis. Strandwitz et al. [30] have examined the polymerization of pyrrole impregnated into mesoporous TiO₂ with the goal to obtain organic-inorganic hybrids. Li et al. [31] have analyzed photopolymerization of diacetylene in the presence of TiO₂ thin films. Ni et al. [32] and Dong and Ni [33] have performed the UVA assisted polymerization of methyl methacrylate in the presence of anatase TiO₂ and P25 TiO₂ particles dispersed in the aqueous monomer solutions. As these studies show, intermediates with high-molecular weight can be formed in photocatalytic experiments. The formation of high molar weight intermediates, as non-volatile polymeric hydrocarbons, apparently took place under UVA illumination of ethylene as in our experiments.



209

210 **Figure 6.** Raman spectra of the black (a) and white (b,c) solid products collected after the
 211 photocatalytic process followed by the photocatalyst heating at 400 °C.

212 The direct analysis of the non-volatile reaction product was complicated by its small surface mass
 213 density. In order to collect this product from the large photocatalyst surface, the heat treatment at
 214 temperature ~400 °C under dry air flow was used. As a result, two kinds of compact solid products
 215 were collected in the reactor output area: black particles and white semi-transparent filaments, which
 216 masses ~0.1-1 mg were sufficient for the Raman analysis. Raman spectra of these products are shown
 217 in Fig. 6. The black product (Fig. 6a) was identified with glassy carbon, which Raman spectrum shows
 218 two characteristic resolved disorder-induced D and first-order allowed G (E_{2g}) bands [34]. The Raman
 219 spectrum of the white product in Fig. 6b shows a complex structure containing multiple vibrational

220 bands; its assignment is less straightforward. Our analysis of available Raman spectra of ethylene and
221 its oxidized and polymerized derivatives brought us to a conclusion about the formation of furan
222 derivatives in the photocatalytic process [35]. In particular, the six observed bands between 900 and
223 1600 cm^{-1} shown in Fig. 6b fit the calculated Raman spectra of oligomers composed of 6 and 8 furan
224 molecules [36]. Moreover, the band at 1730 cm^{-1} identified with the C=O vibration can be observed in
225 polyfuran [37] and indicates the presence of the oxidized derivatives, the best candidate of which is
226 furfural [35]. Because of this, we tentatively assign the deposited product to the furan and/or furfural
227 oligomers (O_N). More evidence to the polyfurfural assignment can provide Raman analysis of the C-H
228 vibration mode in the frequency range of $\sim 3000 \text{ cm}^{-1}$ presented in Fig. 6c. The observed spectral band
229 has partially resolved structure, which belongs to CH groups of the molecule in different geometric
230 positions. Given the structure of the furfural molecule shown in inset of Fig. 6c and tendencies of the
231 frequency evolution [35], the subbands at 2875 cm^{-1} , 2915 cm^{-1} , 2937 cm^{-1} and 2970 cm^{-1} can be
232 respectively assigned to the aldehyde CH stretching (4), antisymmetric and symmetric β -CH stretching
233 (2 / 3) and α -CH symmetric stretching (1) modes. Somewhat lower frequencies of the bands compared
234 to those of the single furfural molecule can be attributed to a partial polymerization leading to the
235 formation of furfural oligomers.

236 As observed in our experiments, the deposited solid products can be removed from the
237 photocatalyst surface by a heat treatment at temperatures $\sim 300 \text{ }^\circ\text{C}$, as show the experimental results of
238 Fig. 2 and Fig. 3. The photocatalyst regeneration could be explained by the oligomers desorption
239 and/or thermal decomposition. In the same time, polyfuran is known to resist temperatures up to
240 400 $^\circ\text{C}$ [37,38], which may explain the successful collection of a small part of this product. Apart of
241 these bands, we observed several narrow peaks at 1041, 1580, 1600 and 1614 cm^{-1} which may be
242 related to C-C vibrations of minor carbonaceous species.

243 According to the above assignment, the photocatalytic oxidation of ethylene results in the
244 formation of short polymeric chains of furan and furfural molecules on the photocatalyst surface. An
245 increase of temperature results in the desorption of larger oligomers and thermal decomposition of
246 smaller ones. The glassy carbon is formed as results of the thermal decomposition. In contrast, the
247 larger polyfurans and polyfurfurals are stable and survive after the thermal desorption. Although we

248 were not optimised the desorption temperature permitting analysis of a full scope of non-damaged
 249 surface products, the collected oligomers Ol_N ($N=6\div 8$) evidences their formation at the photocatalyst
 250 surface as one of major non-volatile products. Since the small Fe(III) doping 0.005 mol% does not
 251 provide any significant modification of the titania band gap energy, surface area, etc. and only
 252 improves the electron-hole separation efficiency [19], we expect the discussed mechanism of the
 253 ethylene decomposition is the general feature of TiO_2 -based photocatalysts.

254

255 3.2 Modeling

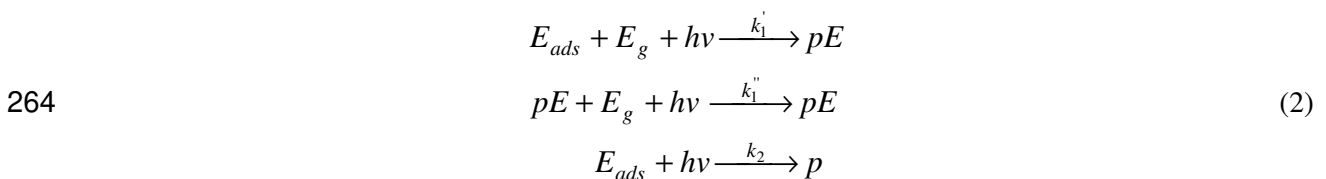
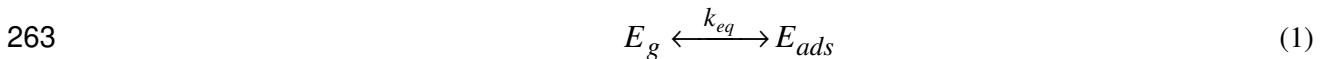
256 In this chapter, a kinetic model is proposed in order to suppose partial polymerisation of ethylene
 257 and formation of oligomers, which do not desorb from the photocatalyst surface. The physical
 258 significations of all introduced parameters were summarized in table 2:

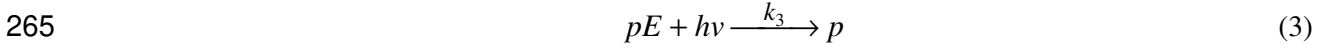
259 Table 2: The physical signification of all introduced parameters

Symbol	Physical signification
E_g/E_{ads}	Gaseous/adsorbed ethylene
pE	Polymeric products
p	Gaseous reaction products (CO_2)
k	Reaction rate constant
n_0	Density per unitary volume of the active TiO_2 surface sites available for adsorption
n	Density per unitary volume of the active TiO_2 surface sites available for ethylene adsorption
m	Density per unitary volume of the active TiO_2 surface sites available for polymeric side products adsorption
y	Ratio between m et n_0
v	Pollutant flow rate through the reactor bed
L	Reactor length (30 cm)
E_a	activation energy

260

261 This process can be triggered by the photogenerated hole transfer to C=C double bonds. Both
 262 adsorbed monomers and oligomers contribute to this process. The relevant reactions are:





266 Where E_g/E_{ads} , pE and p stand for gaseous/adsorbed ethylene, adsorbed polymeric products and
 267 gaseous reaction products (CO_2), which are correspondingly defined as N/n , m and p in the following
 268 equations. The reaction order is 1. It is supposed that the adsorption/desorption process (1) is in
 269 equilibrium while photodecomposition reactions (2) and (3) are not.

270 The ethylene is known to be weakly adsorbed at the TiO_2 surface ($E_a \sim 3$ kcal/mol or $\sim 5kT$ at
 271 room temperature), while the heavy ethylene oligomers are totally adsorbed. Therefore, $n_0 \gg n$
 272 (here n_0 represents the density per unitary volume of the active TiO_2 surface sites available for
 273 adsorption). However, m slowly increases until $m_{t \rightarrow \infty} = n_0$. From (1) it can be obtained:

274
$$n = (n_0 - m) \frac{k_{eq} N}{1 + k_{eq} N} \quad (4)$$

275 The kinetic equation describing (2)-(3) are:

276
$$\frac{dm}{dt} = k_1' n N + k_1'' (1 - m/n_0) m N - k_3 m \quad (5)$$

277
$$\frac{dp}{dt} = k_2 n + k_3 m \quad (6)$$

278 The second term of above Eq. (5) is completed by a factor $(1 - m/n_0)$, which takes into account the
 279 catalyst surface coverage by polymeric products. The equations (4)-(5) can be reduced to

280
$$\frac{dm}{dt} = k_1' n_0 \gamma N + (k_1'' N - k_1' \gamma N - k_3) m - k_1'' N \frac{m^2}{n_0} \quad (7)$$

281 where $\gamma = \frac{k_{eq} N}{1 + k_{eq} N}$.

282 Eq. (7) is solved in approximation of a small coverage of TiO_2 by both monomers and oligomers:
 283 $n_0 \gg n, m$ (we remark that this corresponds to $\gamma \ll 1$). For the sake of simplicity, it is supposed that
 284 the associations “monomer-monomer” and “polymer-monomer” propagate with the same constants
 285 $k_1' = k_1'' \equiv k_1$. Moreover in order to explain the long-lasting accumulation of new species, it is assumed

286 that the polymerisation reaction dominate over the decomposition products formation: $k_1 N \gg k_3$.

287 Then Eq. (7) can be reduced to:

$$288 \quad \frac{dy}{dt} = k_1 N (\gamma + y - y^2) = k_1 N (y - y_1)(y - y_2) \quad (8)$$

289 where $y = m / n_0$ ($y \in [0,1)$) and $y_{1,2} = (1 \pm \sqrt{1 + 4\gamma}) / 2$. Because $\gamma \ll 1$, Eq. (8) can be rewritten as:

$$290 \quad \frac{dy}{dt} = k_1 N (y - 1)(y + \gamma) \quad (9)$$

291 The solution of Eq. (9) is

$$292 \quad m = n_0 \frac{1 - e^{-k_1 N t}}{1 + e^{-k_1 N t} / \gamma} \quad (9)$$

293 In order to obtain the output ethylene concentration, it should consider the pollutants propagation
 294 through the reactor bed. Then the reduction of $N(z)$ is related to the surface sites liberation due to the
 295 decomposition of both ethylene molecules and polymerised chains and it is relate to the rate of the
 296 products exit:

$$297 \quad \frac{dN}{dz} = - \left(\frac{1}{2} \frac{dp}{dt} + \frac{dm}{dt} \right) \frac{dt}{dz} \approx - \frac{1}{2v} \frac{dp}{dt} \quad (10)$$

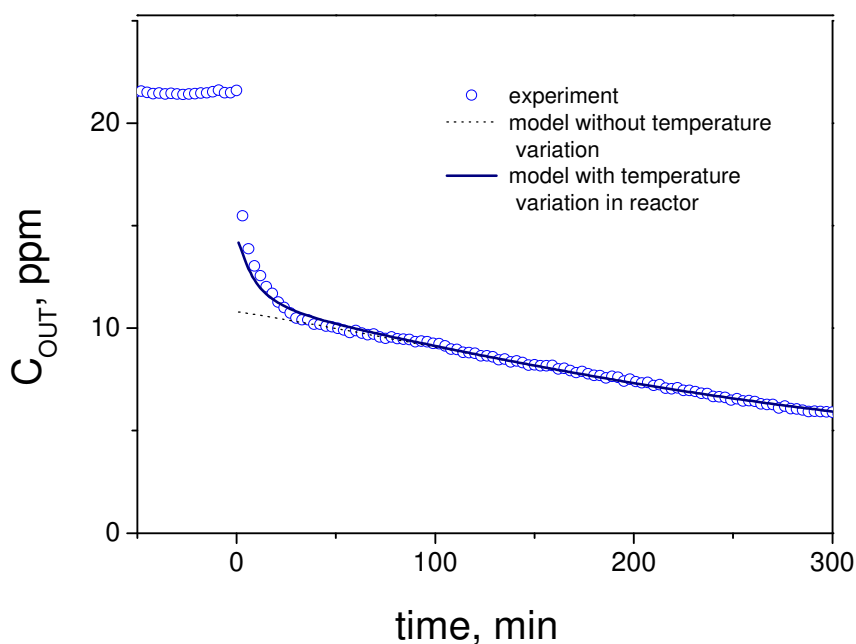
298 where v is the pollutant flow rate through the reactor bed. It is assumed here that dm/dt is a slow
 299 function of time (characteristic time of the polymerisation is ~ 1 hour) while dp/dt is a quick function
 300 of time (characteristic residence time of gas molecules in the reactor bed is ~ 1 s). One can rewrite Eq.
 301 (10) as

$$302 \quad \frac{dN}{dz} = - \frac{1}{2v} (k_2 n + k_3 m) = - \frac{n_0}{2v} [k_2 \gamma + (k_3 - k_2 \gamma) m] \quad (11)$$

303 or

$$304 \quad \frac{dN}{dz} = -\alpha N + (\beta - \alpha N) \frac{1 - e^{-k_1 N t}}{1 + e^{-k_1 N t} / k_{eq} N} \quad (12)$$

305 where $\alpha = k_2 k_{eq} n_0 / 2v$ and $\beta = k_3 n_0 / 2v$ ($0 \leq z \leq L = 30$ cm). Eq. (12) is numerically solved in
 306 order to fit the experimental data with four free parameters α , β , k_1 and k_{eq} . The best fit with $\alpha=0.023$,
 307 $\beta=0.9$, $k_1=0.00055$ and $k_{eq}=0.012$ is shown in Fig. 7 by dotted line.



308

309 **Figure 7.** Ethylene concentration at the photocatalytic reactor exit versus time (experiment and
 310 modelling).

311 The agreement between the model and experiment is good except of the early reaction times.
 312 Since the lamp attains a stationary luminosity within three minutes, the transient period $t \leq 50$ min is
 313 attributed to the activation of photocatalytic reactions. Indeed as the measurements show (Fig. 2), the
 314 reactor temperature increases at this stage.

315 Since the ethylene polymerisation progresses slowly, it is assumed that the ethylene
 316 decomposition is affected by the temperature increase: $k_2 = k_{20} \cdot \exp(E_a / kT)$. The complete least
 317 squared fit of the experimental kinetics with Eq. (12) including $k_2(T)$ with $E_a = 19 \pm 2 \text{ kJ/mol}$ is shown
 318 in Fig. 7 by solid line.

319 The validity of the model assumptions was check in the following section. From the fit, the
 320 equilibrium constant is small indeed. The fit also results in the reaction constants ratio
 321 $k_2 / k_3 = \alpha / \beta k_{eq} \approx 2.1$, which signifies that the photocatalytic decomposition of ethylene is easier
 322 than that of oligomers. One can see that the assumption $k_1 N \ll k_3$ holds, because $k_1 N = 0.0121$ and
 323 $k_3 = 0.9 \cdot 2 \cdot v / n_0 = 580 / n_0 \approx 7 \cdot 10^{-4}$ (gas speed: $v = 30 \text{ cm} / 5.7 \text{ s} = 5.3 \text{ cm/s} = 318 \text{ cm/min}$,

324 $n_0 = m_{TiO_2} S_{BET} / S_{molec} \approx 10^{-2} \cdot 200 / 10^{-19} = 8 \cdot 10^5$ ppm if $m_{TiO_2} = 10^{-2}$ g is used on 30 cm long reactor
325 bed and $S_{molec} = 0.1$ nm²). The photocatalytic process is generally found not very sensitive to
326 temperature with activation energies in the range between 5 and 16 kJ/mol [39]. The apparent
327 activation energy of ethylene degradation over TiO₂ of 13.9-16.0 kJ/mol has been reported by
328 Yamazaki et al.[39]. Our value of E_a fits the upper limit of the earlier reported values. It is concluded
329 that the proposed theoretical model is quite satisfactory.

330 The proposed theoretical model successfully explained the experiment, suggesting polymerisation
331 of ethylene initiated by UVA photons at the photocatalyst surface. In agreement with our previous
332 studies of light-induced processes at the organic-TiO₂ interface, the photogenerated hole can
333 efficiently escape the inorganic solids into surrounding organics[40,41]. Its localisation on a C=C
334 double bond of ethylene molecule will provoke its opening that initiates polymerisation process.

335

336 **IV. Conclusion**

337 In this work the decomposition kinetics of gaseous ethylene onto the optimized Fe(III)-TiO₂
338 anatase photocatalyst with Fe/Ti ratio of 0.005 mol% was studied in a continuous-flow fixed-bed
339 reactor. Based on FTIR, Raman and thermal post-treatment analyses, it was concluded about the
340 formation of a major non-volatile intermediate reaction product in course of the ethylene
341 decomposition, assigned to the oxidized polymeric hydrocarbons: furan and furfural oligomers O_{1N}
342 with N=6÷8. The analysis of the photocatalytic process kinetics showed that this product covers the
343 photocatalyst surface and delays the stationary reaction kinetics.

344 A theoretical model is proposed explaining the process kinetics. The overall photo-assisted
345 process therefore includes two main stages: (i) on the first one, the high-molecular mass product is
346 synthesized enhancing contact with the photocatalyst surface (in contrast to weakly adsorbing ethylene
347 molecules) and (ii) on the second one, the heterogeneous decomposition of the non-volatile species
348 takes place. A weaker rate constant of the oligomers decomposition (as compared with ethylene gas) is
349 compensated by their much stronger adsorption, which enhances the overall reactor yield. The
350 oligomers decomposition can be thermally activated with $E_a=19 \pm 2$ kJ/mol.

351

352 **Acknowledgments**

353 This work is supported by French C'Nano (IdF) network.

354

355

356 References

- 357 [1] U.I. Gaya, A.H. Abdullah, *J. Photochem. Photobiol. C Photochem. Rev.* 9 (2008) 1–12.
- 358 [2] H. Zhang, W. Wang, H. Zhao, L. Zhao, L.-Y. Gan, L.-H. Guo, *ACS Catal.* 8 (2018) 9399–
359 9407.
- 360 [3] J. Ma, H. He, F. Liu, *Appl. Catal. B Environ.* 179 (2015) 21–28.
- 361 [4] S. Sun, J. Ding, J. Bao, C. Gao, Z. Qi, X. Yang, B. He, C. Li, *Appl. Surf. Sci.* 258 (2012)
362 5031–5037.
- 363 [5] Z. Jia, M. Ben Amar, O. Brinza, A. Astafiev, V. Nadochenko, A.B. Evlyukhin, B.N.
364 Chichkov, X. Duten, A. Kanaev, *J. Phys. Chem. C* 116 (2012) 17239–17247.
- 365 [6] Z. Jia, M. Ben Amar, D. Yang, O. Brinza, A. Kanaev, X. Duten, A. Vega-González, *Chem.*
366 *Eng. J.* 347 (2018) 913–922.
- 367 [7] X. Chen, R. Li, X. Pan, X. Huang, Z. Yi, *Chem. Eng. J.* 320 (2017) 644–652.
- 368 [8] X. Liang, P. Wang, M. Li, Q. Zhang, Z. Wang, Y. Dai, X. Zhang, Y. Liu, M.H. Whangbo, B.
369 Huang, *Appl. Catal. B Environ.* 220 (2018) 356–361.
- 370 [9] N. Pathak, O.J. Caleb, M. Geyer, W.B. Herppich, C. Rauh, P. V. Mahajan, *Food Bioprocess*
371 *Technol.* 10 (2017) 982–1001.
- 372 [10] D.-R. Park, J. Zhang, K. Ikeue, H. Yamashita, M. Anpo, *J. Catal.* 185 (1999) 114–119.
- 373 [11] S. Yamazaki, S. Tanaka, H. Tsukamoto, *J. Photochem. Photobiol. A Chem.* 121 (1999) 55–61.
- 374 [12] K. Bhattacharyya, S. Varma, K. Kishore, N.M. Gupta, *Res. Chem. Intermed.* 32 (2006) 17–30.
- 375 [13] W.-D. Wang, A. Bakac, J.H. Espenson, *Inorg. Chem.* 34 (1995) 6034–6039.
- 376 [14] H. Einaga, Y. Teraoka, *Res. Chem. Intermed.* 34 (2008) 617–628.
- 377 [15] G.Y. Popova, T. V. Andrushkevich, Y.A. Chesalov, E.S. Stoyanov, *Kinet. Catal.* 41 (2000)
378 805–811.
- 379 [16] B. Hauchecorne, T. Tytgat, S.W. Verbruggen, D. Hauchecorne, D. Terrens, M. Smits, K.
380 Vinken, S. Lenaerts, *Appl. Catal. B Environ.* 105 (2011) 111–116.
- 381 [17] M. Anpo, K. Chiba, M. Tomonari, S. Coluccia, M. Che, M.A. Fox, *Bull. Chem. Soc. Jpn.* 64
382 (1991) 543–551.
- 383 [18] S. Tieng, R. Azouani, K. Chhor, A. Kanaev, *J. Phys. Chem. C* 115 (2011) 5244–5250.

- 384 [19] S. Tieng, A. Kanaev, K. Chhor, *Appl. Catal. A Gen.* 399 (2011) 191–197.
- 385 [20] Y. Ichihashi, Y. Matsumura, *Res. Chem. Intermed.* 29 (2003) 891–896.
- 386 [21] V. Keller, P. Bernhardt, F. Garin, *J. Catal.* 215 (2003) 129–138.
- 387 [22] G. Pecchi, P. Reyes, T. López, R. Gómez, A. Moreno, J.L.G. Fierro, A. Martínez-Arias, *J. Sol-*
388 *Gel Sci. Technol.* 27 (2003) 205–214.
- 389 [23] M. Benmami, K. Chhor, a V Kanaev, *J. Phys. Chem. B* 109 (2005) 19766–71.
- 390 [24] B. Hauchecorne, D. Terrens, S. Verbruggen, J.A. Martens, H. Van Langenhove, K.
391 Demeestere, S. Lenaerts, *Appl. Catal. B Environ.* 106 (2011) 630–638.
- 392 [25] W. Sawodny, K. Niedenzu, J.W. Dawson, *Spectrochim. Acta Part A Mol. Spectrosc.* 23 (1967)
393 799–806.
- 394 [26] G.Y. Popova, T. V. Andrushkevich, Y.A. Chesalov, E.S. Stoyanov, *Kinet. Catal.* 41 (2000)
395 805–811.
- 396 [27] M. Anpo, K. Chiba, M. Tomonari, S. Coluccia, M. Che, M.A. Fox, *Bull. Chem. Soc. Jpn.* 64
397 (1991) 543–551.
- 398 [28] I.G. Popović, L. Katsikas, H. Weller, *Polym. Bull.* 32 (1994) 597–603.
- 399 [29] C. Damm, D. Völtzke, H.-P. Abicht, G. Israel, *J. Photochem. Photobiol. A Chem.* 174 (2005)
400 171–179.
- 401 [30] N.C. Strandwitz, Y. Nonoguchi, S.W. Boettcher, G.D. Stucky, *Langmuir* 26 (2010) 5319–
402 5322.
- 403 [31] L. Li, Y. Wang, F. Yan, L.A. Samuelson, J. Kumar, *J. Macromol. Sci. Part A* 47 (2010) 1161–
404 1166.
- 405 [32] X. Ni, J. Ye, C. Dong, *J. Photochem. Photobiol. A Chem.* 181 (2006) 19–27.
- 406 [33] C. Dong, X. Ni, *J. Macromol. Sci. Part A* 41 (2004) 547–563.
- 407 [34] Y. Wang, D.C. Alsmeyer, R.L. McCreery, *Chem. Mater.* 2 (1990) 557–563.
- 408 [35] T. Kim, R.S. Assary, L.A. Curtiss, C.L. Marshall, P.C. Stair, *J. Raman Spectrosc.* 42 (2011)
409 2069–2076.
- 410 [36] C. Liu, J. Zhang, G. Shi, Y. Zhao, *J. Phys. Chem. B* 108 (2004) 2195–2199.
- 411 [37] X.G. Li, Y. Kang, M.R. Huang, *J. Comb. Chem.* 8 (2006) 670–678.

- 412 [38] G. Tourillon, F. Garnier, *J. Electroanal. Chem. Interfacial Electrochem.* 135 (1982) 173–178.
- 413 [39] A. Mills, S. Le Hunte, *J. Photochem. Photobiol. A Chem.* 108 (1997) 1–35.
- 414 [40] A. Uklein, P. Gorbovyi, M. Traore, L. Museur, A. Kanaev, *Opt. Mater. Express* 3 (2013) 533.
- 415 [41] A.I. Kuznetsov, O. Kameneva, N. Bityurin, L. Rozes, C. Sanchez, A. Kanaev, *Phys. Chem.*
- 416 *Chem. Phys.* 11 (2009) 1248.
- 417

UV + Fe-TiO₂

